J. COMBIN. MATH. COMBIN. COMPUT. 127b (2025) 3443--3461

Journal of Combinatorial Mathematics and Combinatorial Computing
www.combinatorialpress.com/jcmcc

A finite element analysis-based study of the effects of biomechanical characteristics on instructional interventions in sports

Rui Zhang[1], Zhe Shao[2,✉]

[1] College of Sciences, North China University of Technology, Beijing, 100144, China
[2] Sports-Department, Beijing Technology and Business University, Beijing, 100048, China

ABSTRACT
In this paper, finite element analysis is applied to the mechanical characterization of the foot. A finite element simulation model of the foot is constructed and its material properties are defined. Finite element analysis is applied to calculate the stresses on various tissues of the foot under different touchdown modes. Set up controlled experiments to verify the advantages of FEA technology in sports. The material property values of each tissue in the simulation model differed greatly, which was in line with the actual situation of biological tissues. In the 2 touchdown modes, the change curves of flexion and extension angles of the supporting foot were generally similar in the latter 75% of the supporting phase, and the differences were concentrated in the first 25%. The movement of the foot on the coronal plane showed a general tendency toward eversion. There were 2 peaks in the vertical ground reaction force variation in the heel-touch mode and only 1 peak in the non-heel-touch mode. The resistance impulse and power impulse ratios varied widely. The time of occurrence of the maximum contact stress on the talo-heel joint surface varied. P<0.05, the experimental group was better than the control group in terms of skill level, learning interest and initiative of the two groups of students after the experiment. The use of finite element analysis to assist physical education teaching can enhance students' enthusiasm and skill level.

Keywords: biomechanical characteristics, finite element analysis, simulation model model, touching pattern, physical education and sports

1. Introduction

The concept of sports biomechanics was proposed in the 1960s, but the practical application of sports biomechanics, with its impact on various activities in sports, biology, physics and other disciplines has

✉ Corresponding author.
E-mail address: brackzr@ncut.edu.cn (Z. Shao).
Received 05 March 2024; Revised 20 June 2024; Accepted 15 November 2024; Published Online 16 April 2025.
DOI: 10.61091/jcmcc127b-192

long existed [1]. On the basis of fully studying and analyzing sports biomechanics, comprehensively and reasonably utilizing the research results of sports biomechanics and applying them in the teaching and research work of various disciplines related to it will greatly enhance the research efficiency of the relevant work, thus improving the research level [2-4]. Therefore, sports biomechanics is a modern and comprehensive discipline in line with the development of the times, which is worthy of everyone's research and study [5].

The application of sports biomechanics is mainly in physical education, sports and other aspects, and sports are divided into mass sports and competitive sports. The main purpose of the study of popular sports is to improve the physical quality of the practitioners, prevent human diseases, enhance the immunity of the body of the exerciser, prevent sports injuries to human organs, and reduce the emergence of "occupational diseases" and so on [6-8]. After the application of sports biomechanics in popular sports disciplines, it has greatly improved the physical quality of the general public, and promoted the enhancement and improvement of the essence, qi and spirit of all people [9-11]. In terms of competitive sports, with the increase in popularity and development of sports worldwide, sports have become more and more one of the important standards to measure the comprehensive national power of a country [12-13]. And in order to train competitive sports athletes more professionally and effectively, protect the personal safety of athletes and improve the level of competitive sports in China, it is necessary to include comprehensive, scientific, rational and practical sports biomechanics [14-16]. The discipline of sport biomechanics, as a comprehensive research discipline, its main research population and backbone should be the majority of students and teachers in colleges and universities [17]. However, at present, many universities in China still do not pay attention to the development of sports biomechanics in sports teaching, which seriously hinders the long-term development of the field of sports mechanics and physical education in China [18-20].

In this paper, we study the mechanical characteristics of the foot and the specifics of the computational formula of finite element analysis, combine the two, and apply them in the analysis of the foot force of athletes in sports teaching. The 3D modeling software was used to initially establish the skeletal model of the foot and ankle. The ligaments and metatarsal fascia of the foot were further modeled to improve the skeletal model of the foot and ankle. Define the material properties of each tissue in the foot and ankle skeletal model to ensure that the model class has significant biological characteristics. Analyze the changes of ankle joint angle, ground reaction force, and contact stress of the talo-heel joint surface in heel-touch and non-heel-touch modes. To investigate the effectiveness of finite element analysis technology in sports to assist teaching through controlled experiments. Distribute questionnaires to investigate the role of FEA techniques in enhancing students' attitudes toward sports.

2. Integration of finite element analysis and mechanical characterization of the foot

To analyze the changes of foot mechanical characteristics of athletes in the process of sports, to study the steps of derivation and the scope of application of the computational formula of finite element analysis, and to lay a solid foundation for the subsequent construction of foot simulation models and calculation of change trends.

2.1. Mechanical characteristics of the foot

2.1.1. Kinematics of the foot. Foot movements are complex with three axes of motion and three planes of motion. Movements in the sagittal plane include dorsiflexion and plantarflexion, movements in the coronal plane include inversion and eversion, and movements in the horizontal plane include abduction and adduction. The subtalar joint is composed of the corresponding articular surfaces of the talus and the heel bone, and its pre-rotation and post-rotation are generally used to describe the position of the metatarsal surfaces. The pronated metatarsal surfaces face outward in a combination of dorsiflexion, valgus, and abduction movements; the pronated metatarsal surfaces face inward in a combination of ankle plantarflexion, valgus, and adduction movements. The movements of the toes include flexion, extension, adduction, and abduction.

2.1.2. Foot dynamics. The foot is subjected to considerable ground reaction forces during movement. The PvGRF sustained during walking is approximately 1.3 BW, while running can reach 2.76 BW, and during vertical jump landings can reach 3.6-7.1 BW. for complex gymnastics aerial skill landings, there is a much greater PvGRF. gymnasts landed with a forward flip with a PvGRF ranging from 7.5-15.7 BW, and backward flips ranging from 7.2-13.3 Bw. In the plantar pressure test, participants were asked to stand barefoot and found that the plantar pressure distribution was characterized as follows: heel 61%, midfoot 7%, forefoot 27%, and toes 5%.

The soft tissues and arches of the foot provide cushioning for the foot and protection for internal structures. The bones of the foot and their joint structures form the “bow” of the arch, while the plantar fascia and tendons form the “string” of the arch. The skin of the sole of the foot is tightly attached to the basal bones, joints and tendon sheaths through the plantar fascia. When the metatarsophalangeal joints are extended, the metatarsophalangeal fascia restricts the movement of the plantar fat pad (heel pad). Furthermore, the heel pad is a high sole specialization that cushions shock. This combination of the “arch”, “strings”, and heel pad cushions and dampens the foot during walking, running, jumping, and landing.

2.2. Research on Finite Element Analysis Methods

2.2.1. Derivation of computational equations. A piece of hollow kinematic surface without surface skin is designed, and the required kinematic surface computational unit, i.e., the structure containing the upper and lower tibial fibulae and the membranous ligaments, is extracted. It is assumed that (1) the structure is continuous and the shape of the tibial cross-section is constant; (2) the point of inversion of the upper and lower tibial fibulae is at their midpoints; (3) the computational equation is used for structural meshes larger than 5; (4) torsional deformations are ignored; and (5) the cross-sectional area of the lower tibial fibulae is always higher than that of the upper tibial fibulae.

A projection of this structure in the zy-plane under the Cartesian coordinate system yields a planar figure. This projection is first equated to a planar tibia of the same length and height. In order to obtain the relationship between the upper and lower tibiofibular end loads Q_1 and Q_2 and the equivalent load Q (loads Q, Q_1, and Q_2 are calculated in Newtons per unit width (N/m)), a set of symmetric loads Q_1, Q_2, and the opposite unit loads are applied to the upper and lower tibiofibular ends of this projected structure, and a bending moment image of the structure is obtained.

Using the graph multiplication method, the graph multiplication of the bending moment image and the unit ligament image yields an expression for the end displacement δ of the membranous ligament:

$$\begin{aligned}\delta = &\frac{1}{E_1 I_1}\left[\frac{1}{2}\cdot\frac{abQ_1}{2}\cdot\frac{a}{2}\cdot\frac{2}{3}\left(-\frac{a}{2}\right)\right]+\frac{1}{E_3 I_3}\left(\frac{1}{2}\cdot\frac{abQ_2}{2}\cdot\frac{a}{2}\cdot\frac{2}{3}\cdot\frac{a}{2}\right)\\ &+\frac{1}{E_2 I_2}\left\{\left(\frac{1}{2}\cdot abQ_2\cdot\frac{bhQ_2}{b(Q_1+Q_2)}\cdot\frac{a}{2}\right)+\left[\frac{1}{2}\cdot abQ_1\cdot\frac{bhQ_1}{b(Q_1+Q_2)}\left(-\frac{a}{2}\right)\right]\right\}\end{aligned} \tag{1}$$

where: E_i - the modulus of elasticity of the material of the member ($i=1,2,3$; 1 is the upper tibial fibula, 2 is the membranous ligament, and 3 is the lower tibial fibula, below);

I_i - moment of inertia of the ligament;

z_i - height of the ligament;

a - length of the side of the kinematic surface calculation grid;
b - width of the tibiofibular section;
h - the height of the kinematic plane calculation grid.

The equation of quantitative relationship between Q_l and Q_2 is obtained by making the end shift δ equal to zero:

$$Q_1 = \beta Q_2 \tag{2}$$

where β is called the stiffness control parameter of the kinematic surface and is of the form:

$$\beta = \frac{a/6E_3I_3 + h/E_2I_2}{a/6E_1I_1 + h/E_2I_2} \tag{3}$$

Then, according to the balance of forces on the moving surface, neglecting the two wings of the x-direction part and considering the equivalent width of the equivalent tibia fibula a, we get the relationship equation between the equivalent load Q and Q_1, Q_2:

$$bQ_1 + bQ_2 = aQ \tag{4}$$

Combinatorial equation (2) i.e., performance:

$$Q = \frac{(\beta+1)b}{a\beta}Q_1; Q = \frac{(\beta+1)b}{a}Q_2 \tag{5}$$

According to the moment balance equation for the equivalent tibial fibula it can be obtained that O is the equivalent load on the upper side of the equivalent tibia:

$$bOh - bQa = 0 \tag{6}$$

Solution:

$$O = \frac{aQ}{h} \tag{7}$$

Returning to the spatial coordinate system, it is again assumed that the upper and lower tibial fibulae on the lateral side of the hollow kinematic plane are not involved in out-of-plane shear, load $f=0$, from which load $F=0$ can be obtained. The equivalent tibial fibulae are then scaled up into a homogeneous body. According to Eq. (4) and Eq. (7), the contact stress of this equivalent homogeneous body can be obtained:

$$\tau_{zy} = \frac{O}{a} = \frac{Q}{h} \tag{8}$$

$$\tau_{yz} = \frac{aQ}{ah} = \frac{Q}{h} \tag{9}$$

Eqs. (8) and (9) are consistent with the contact stress reciprocity theorem. The strain energy is then calculated from the contact stresses of the equivalent homogeneous body:

$$U_{yz}^e = \int \frac{\tau^2}{2G}dV = \frac{a^2Q^2}{2G^e h} \tag{10}$$

Eq. (10) takes into account the effect of the Poisson's ratio of the material, which is expressed in the kinematic plane as:

$$G_i = \frac{E_i}{2(1+v_i)}(i=1,2,3) \tag{11}$$

Similarly to Eq. (10), the strain energy of the original kinematic surface structure is:

$$U_{yz}=\int\frac{\tau^2}{2G}dV=\frac{Q_1^2}{z_1^2}\left[\frac{z_1b(2a-b)}{2G_1}+\frac{b^2z_2}{2G_2}\right]+\frac{Q_2^2}{z_3^2}\left[\frac{z_3b(2a-b)}{2G_3}+\frac{b^2z_2}{2G_2}\right] \tag{12}$$

According to the functional principle, make

$$U_{yz}=U_{yz}^e \tag{13}$$

Solve the equation for the out-of-plane equivalent contact modulus of the moving surface:

$$G^e=\frac{b(\beta+1)}{h\left[\frac{\beta^2}{z_1}\left(\frac{2a-b}{G_1}+\frac{bz_2}{G_2z_1}\right)+\frac{1}{z_3}\left(\frac{2a-b}{G_1}+\frac{bz_2}{G_2z_3}\right)\right]} \tag{14}$$

2.2.2. Computational applicability analysis. The equation for the out-of-plane equivalent contact modulus of the kinematic surface needs to be coupled with equivalent loads in order to calculate the joint shear strain. From the derivation process in the previous section, it can be seen that Eq. (14) holds when the upper and lower tibiofibular end loads Q_1 and Q_2 of the kinematic plane are equal in number and when the upper and lower tibiofibular cross-sectional shapes and the material strengths are the same, which is embodied in this case:

$$\frac{Q_1}{Q_2}=1;\beta=1 \tag{15}$$

In this case it is considered feasible to directly use the computational equation (14) and the equivalent load equation (5) for the shear strain gauging of the kinematic surfaces, which is also a relatively common practical structural design and use condition, and is defined as Case 1.

However, in the process of using the proposed plate method, we need to calculate the upper and lower tibial fibula of the kinematic surface of different shapes: the upper tibial fibula considering the existence of the surface skin, its height z_1 is always lower than that of the lower rib height z_2; in the actual engineering, the upper and lower tibial fibula of the material strength is different; the upper and lower tibial fibula are subjected to different values of loads. Whether Eq. (14) can be adapted to situations other than Case 1 needs to be verified. So, let a similar situation arise and the stiffness control parameters of the kinematic surfaces are then embodied as:

$$\beta=\frac{a/6E_3I_3+h/E_2I_2}{a/6E_1I_1+h/E_2I_2}\neq 1 \tag{16}$$

From Eq. (16), due to the change of the upper and lower tibial fibers, the stiffness control parameter of the kinematic surface is no longer equal to 1. The relationship between the actual load and the equivalent load of the kinematic surface is no longer equal, and Eq. (5) is no longer applicable. It is necessary to re-establish the relationship between the actual load and the equivalent load, and the relationship between the actual load and the stiffness control parameter is obtained by shifting the terms:

$$\frac{Q_1}{Q_2}=\beta \tag{17}$$

At this time, we observe equation (17), and get three kinds of cases when this equation is not equal, that is: 1) the actual load of upper and lower tibia and fibula is the same, and the stiffness control parameter is not 1; 2) the actual load of upper and lower tibia and fibula is different, and the stiffness control parameter is 1; 3) the actual load of upper and lower tibia and fibula is different, and the stiffness control parameter is not 1 either.

Define case 2, i.e., the actual loads on the upper and lower tibial fibula are the same and the stiffness control parameter is not 1. In this case, Eq. (17) becomes the following form:

$$\frac{Q_1}{Q_2}=1; \beta \neq 1 \tag{18}$$

In order to satisfy the correlation with β while satisfying $Q_1 = Q_2$, the loading component is corrected by adding a correction factor of α:

$$\alpha \frac{Q_1}{Q_2}=\beta \tag{19}$$

The value of correction factor α can be solved for:

$$\alpha=\beta \tag{20}$$

Correct Q_1 with correction factor α and then obtain the corrected equivalent load relationship equation from Eq:

$$Q^2=\frac{(\beta+1)b}{a\beta}\alpha Q_1 \tag{21}$$

Define case 3, i.e., the actual loads on the upper and lower tibial fibers are different and the stiffness control parameter is 1. In this case, Eq. (17) becomes the following form:

$$\frac{Q_1}{Q_2}\neq 1; \beta=1 \tag{22}$$

At this point by the equation (3) will get two unequal equivalent loads, do not meet the calculation requirements. Instead, a new equivalent load Q^3 can be obtained from the equilibrium equation:

$$Q^3=\frac{b\left(Q_1+Q_2\right)}{a} \tag{23}$$

Defining case 4, the actual loads on the upper and lower tibial fibers are different and the stiffness control parameter is not 1. In this case, Eq. (17) takes the following form:

$$\frac{Q_1}{Q_2}\neq \beta \neq 1 \tag{24}$$

At this point, the original equivalent load relationship has been destroyed, and only Eq. (23) can be used to calculate the current equivalent load calculation.

3. Finite element simulation modeling of the foot

Through the steps of "establishing foot simulation model - mesh division - material property definition - feature change calculation - visualization analysis", the finite element analysis method transforms the complex mechanical features of the foot in the process of movement into computable mathematical problems. It helps physical education teachers to observe the athletes' movements more carefully, especially the trajectory of the foot movement from the ground to the ground, so as to provide the athletes with fine and personalized sports interventions in a timely manner.

3.1. Skeletal modeling of the foot and ankle

3.1.1. Foot and Ankle Skeletal Model Pretreatment. STP files of each foot and ankle bone model and soft tissue model of the athlete in sports were imported into the 3D modeling software. After importing the model (tibial cortical bone, for example), the integrity of the ankle skeleton model was checked to see if there were any fragments of bones that were connected to each other, which were caused by small fragments left over from the previous processing, by selecting all the bones and then choosing to invert the selection, and then deleting the parts that were not connected to the bones. In the polygon toolbar, select Remesh to ensure that the bones have a regular mesh, which will ensure the validity of subsequent operations. After remeshing, click Remove All Boundaries to ensure that the bone has no unnecessary boundaries. Next, use the Remove Staples, Sculpting Knife, and Remove Features tools to remove the remaining roughness of the bone to ensure that the bone is smooth and simulated. When utilizing these tools, care should be taken to avoid overdoing it and losing the original corridors and surfaces of the bone. After smoothing the bone, we can use the mesh doctor function to check the processed model. If the model has problems such as small holes, channels, or spikes, the model will be corrected manually, or through the one-click repair function. The holes or channels in the model, if not treated, will cause errors when the next software operation is performed resulting in the experiment not being able to proceed further.

After smoothing and processing the ankle bone model, we need to convert it into a polysurface polygon. Click on the "Accurate Surfaces" function in the software, select the appropriate curvature sensitivity for the bone in "Explore Contours", and then use the Brush, Lasso, and other buttons to construct the contour lines for our target bone. The purpose of the contour lines is to create a surface piece for the next step, so we need to draw the contour lines in the areas of the bone that have large curvature or bulges. Once the contour lines have been constructed, we need to click Edit Contour Lines to correct the contour lines where there are obvious bifurcations or distortions. After fixing the contour lines, we need to construct the curved surface pieces of the bone according to the size of the bone. The number of curved surface pieces is not standardized and needs to be adjusted according to the size of the bone. Then we need to click on "Construct Grid" to double-check the model for errors such as missing or intersecting surfaces, and then make further adjustments based on the errors. After we have completed these steps, we click "Fit Surface" to get a smooth and structurally complete bone model. The rest of the bone and soft tissue models will be modeled according to the above steps.

After completing the above steps, we get the cortical bone of each processed bone. The complete foot and ankle joint complex model also needs to construct the cancellous bone model of the tibia and fibula. The difference between the cancellous bone model and the cortical bone model is that the cancellous bone needs to be processed by the "offset" function at the very beginning. In this experiment, the cancellous bone was offset inward by 0.5 mm, and after the offset was completed, the cancellous bone model only needed to follow the cortical bone model in order. After completing the processing of the model including cancellous bone, cancellous bone and soft tissue model, the model format was saved as STP format in turn.

3.1.2. Establishment of foot ligaments as well as the metatarsal fascia. After pre-processing the model, an overall skeletal model of the foot and ankle is initially obtained. The foot ligaments and metatarsal fascia were further modeled to obtain a complete finite element simulation model of the foot. In this paper, based on the anatomical and structural characteristics of the foot ligaments and MRI imaging data, combined with the three-dimensional anatomical information of the ligaments (including the starting and ending points of the ligaments and the direction of the ligaments) in the Primal Pictures of the finite element platform 0vidSP, a comprehensive consideration was made to obtain a complete simulation model of the ankle. The ligaments (including the starting and ending points of the ligaments as well as their directions) in the "Interactive foot and ankle" in Primal Pictures on the Finite Element Platform 0vidSP were modeled. Table 1 shows the ligament details. The specific modeling method was based on the Truss (T3D2) unit in the finite element platform ABAQUS to model 133 ligaments, and a total of 136 Truss units were created.

Table 1. Ligaments included in the finite element model of foot and ankle

Name	Owning joint	Quantity	Name	Owning joint	Quantity
Lateral collateral ligament interphalangeal	Interphalangeal joints	17	Ligamenta calcaneocuboideum dorsalis	Calcaneocuboid joint	2
Dorsal phalangeal ligament	Interphalangeal joints	9	Plantar calcaneocuboid ligament	Calcaneocuboid joint	2
Plantar ligament of phalanges	Interphalangeal joints	9	Long plantar ligaments	Calcaneocuboid joint	5
Collateral ligaments of metatarsophalangeal joint	Metatarsophalangeal joint	11	Diverge ligamenta calcaneocuboideum	Calcaneocuboid joint	2
Plantar ligaments of metatarsophalangeal joint	Metatarsophalangeal joint	6	Anterior talar ligament	Talocalcaneal joint	2
Deep transverse ligament of metatarsal base	Metatarsophalangeal joint	5	Ligamenta talocalcaneus posterior	Talocalcaneal joint	2
Ligamenta metatarsalis dorsalis	Intermetatarsal joint	4	Medial talocalcaneal ligament	Talocalcaneal joint	2
Plantar metatarsal ligament	Intermetatarsal joint	4	Lateral talocalcaneal ligament	Talocalcaneal joint	2
Ligamenta tarsometatarsus dorsalis	Tarsometatarsal joint	8	Ligamenta cuboscaphoid dorsalis	Navicuboid joint	2
Plantar tarsometatarsal ligament	Tarsometatarsal joint	5	Plantar cuboscaphoid ligament	Navicuboid joint	2
Ligamenta cuneocuboideum dorsalis	Cuneocuboid joint	2	Ligamenta talocalcaneum interosseum	Articulation talocalcaneonavicular	2
Plantar cuneocuboid ligament	Cuneocuboid joint	2	Calcaneonavicular plantar ligament	Articulation talocalcaneonavicular	2
Dorsal intercuneiform ligament	Intercuneiform joint	3	Ligamenta divergences	Articulation talocalcaneonavicular	3
Plantar intercuneiform ligament	Intercuneiform joint	2	Ligamenta talonavicularis dorsalis	Articulation talocalcaneonavicular	2
Ligamenta cuneonavicularis dorsalis	Cuneonavicular joint	4	Plantar fascia		6
Plantar cuneonavicular ligament	Cuneonavicular joint	4			

3.1.3. Definition of Material Properties of the Organizational Structures of the Foot and Ankle. The selection of appropriate materials defines each tissue structure in the foot and ankle skeletal model to make the model more compatible with the real biological tissues. Table 2 shows the material parameters and unit types. Usually, the stress-strain relationship of biological tissues under different loads has the characteristics of nonlinearity and hyperelasticity, which belongs to anisotropic nonlinear objects, and the basic research of such tissue materials is difficult, and it is not easy to obtain the accurate parameters from mechanical experiments. Therefore, most of the current biomechanical finite element simulation analyses of bones are based on the assumption of isotropic, homogeneous and continuous linear elastic body. Therefore, in this study, in addition to the peripheral soft tissue, Springs unit, other tissue materials are approximated as linear elastic materials, and the relevant material parameters and unit types are selected as general research parameters. Analyzing Table 2, there are four types of unit types with large differences in elastic modulus.

Table 2. Material parameters and cell types

Name	Cell type	E(MPa)	Poisson's ratio v	Cross-sectional area (mm^2)
Foot skeleton	3D-Tetrahedra	7400	0.4	-
Fibula	3D-Tetrahedra	7400	0.4	-
Tibial cortex	3D-Tetrahedra	20035	0.415	-
Cancellous bone of tibia	3D-Tetrahedra	446	0.4	-
Peripheral soft tissue	3D-Tetrahedra	Hyperelastic	-	-
Foot ligament	Tension-only-Truss	261	-	18.5
Aponeurosis plantaris	Tension-only-Truss	351	-	58.7
Gristle	3D-Tetrahedra	1	0.5	-
Support plate	3D-Brick	17001	0.2	-

The material properties of the ankle ligament, the lower tibiofibular joint ligament, and the interosseous membrane of the lower leg were determined separately, taking into account the objective anatomical and mechanical differences between the different ligaments. Table 3 shows the specific data on the stiffness values of each ligament material in the model for the medial and lateral ankle and the lower tibiofibular. Observing the corresponding data, the stiffness values of each ligament material of the inner, outer ankle and lower tibiofibular ligaments in the model ranged from 39.2 N/mm to 90102 N/mm, with a large difference in stiffness between each ligament material, which is consistent with the real foot ligament situation.

Table 3. Stiffness values of each ligament in the model

Medial, lateral malleolus and inferior tibiofibular ligaments	Stiffness (N/mm)
Scaphotibial ligament	39.2
Anterior talotibial ligament	122.7
Calcaneotibial ligaments (2 pieces)	63.1
Ligamenta talotibialis posterior (4 pieces)	60.1
Posterior talofibular ligament (2 pieces)	82.2
Calcanefibular ligament	126.7
Anterior talofibular ligament	141.9
Anterior inferior tibiofibular ligaments (2 pieces, proximal and distal)	9079
Inferior tibiofibula interosseous ligaments	235
Inferior posterior tibiofibular ligaments (2 pieces, proximal and distal)	90102
Lower leg interosseous membrane (2 pieces)	401

3.2. Foot kinematics and dynamics of different touchdown patterns

Six representative athletes were invited to participate in the foot movement test, and their foot movement images and data were collected to establish the foot and ankle skeletal model for the feature operation and visualization study of finite element analysis according to the steps in 3.1. No significant differences were observed in the temporal and spatial parameters of the six athletes in one complete gait cycle under both heel touchdown mode (RFS) and non-heel touchdown mode (NRFS) touchdown modes. The gait cycle duration: 0.66±0.15 s in RFS and 0.61±0.03 s in NRFS; step length: 2.48±0.17 m and 2.33±0.08 m in RFS and NRFS, respectively; and the mean of the duration of the support phase/duration of the vacated phase: 0.51 in RFS and 0.53 in NRFS.According to the foot surface area

(FSA) calculations, six subjects completed both the RFS and NRFS test maneuvers.The FSA of the six subjects in the RFS jog was 14.85 ± 5.17°. In the completed NRFS run, the FSA was 2.20 ± 4.05°.

3.2.1. Ankle angle. Figure 1 shows the ankle joint angle changes in the support phase of the right foot under two touchdown modes. Comparison of the angular change curves of the ankle joint of the supporting side in the sagittal plane under the two different touchdown modes revealed that the angular change curves of foot flexion and extension of the supporting foot in the posterior 75% of the supporting phase were generally similar in the two different touchdown modes: whether the RFS or NRFS mode was used. The differences in ankle angle changes in the sagittal plane between the two modes of touchdown were mainly found in the first 25% of the support phase. In the NRFS pattern, the majority of subjects' feet were in plantarflexion at the moment of touchdown, with a gradual transition from plantarflexion at touchdown to dorsiflexion over the period from the beginning of touchdown to about 25% of the support phase. In the RFS mode, the foot transitioned from dorsiflexion to maximal dorsiflexion at the beginning of touchdown and then to plantarflexion until it left the ground. The range of motion of the ankle joint of the supporting foot in the sagittal plane was similar in both touchdown modes, with an average range of motion of 39.80° in RFS and 38.67° in NRFS.

The overall trend of foot motion in the coronal plane in both touchdown modes showed a tendency toward eversion.The greater difference in foot motion in the coronal plane in the NRFS suggested a greater interindividual variation in foot motion in the coronal plane when completing the NRFS run.The foot began to invert at approximately 91% of the end of the support phase in the RFS, whereas this feature appeared to be present in the 65% of the support getting along in the NRFS mode.The supported foot in the NRFS mode had a The average maximum inversion angle in the NRFS pattern was 7.54°. Compared with the RFS, the midfoot in the support phase of the NRFS showed a longer and more angular inversion in the coronal plane.

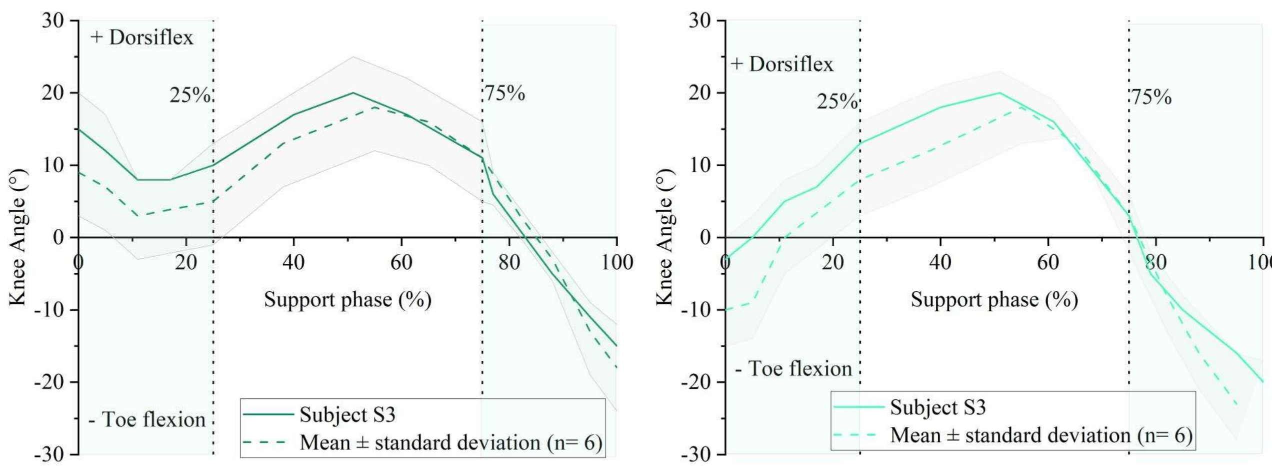

(a) Flexion and extension trend of RFS foot

(b) Flexion and extension trend of NRFS foot

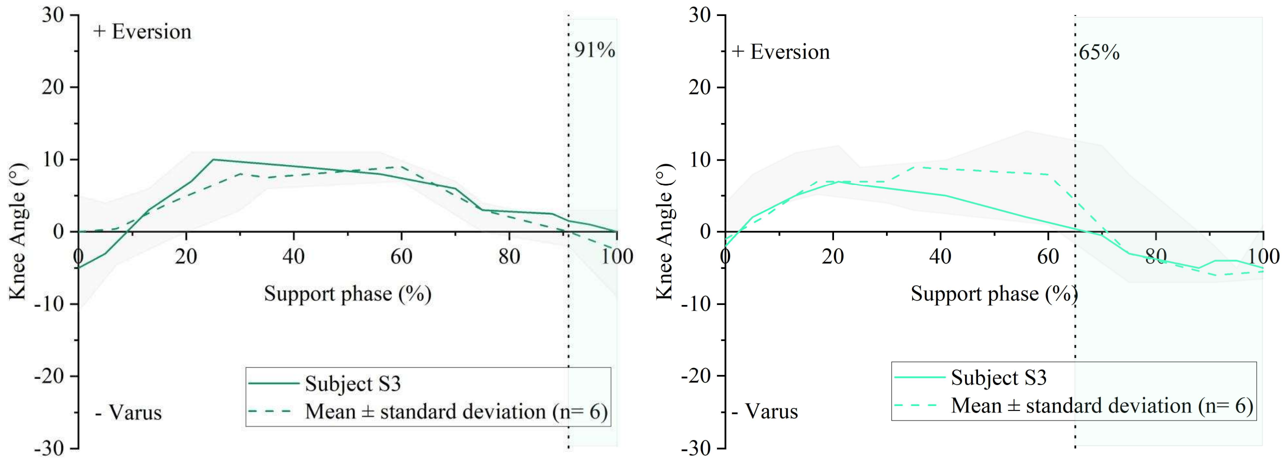

(c) The trend of foot and foot eversion in RFS (d) The trend of foot and foot eversion in NRFS

Fig. 1. Ankle joint Angle of the right foot support phase in both modes

3.2.2. Ground reaction forces. Ground reaction force over time (GRF) curves of one subject were selected to compare the characteristics of their changes in the two touchdown modes. The ankle joint range of motion of this subject was within one times the standard deviation of the overall sample, and the ankle joint angle and GRF changes were used to represent the movement characteristics of the six subjects in completing the jogging in different touchdown modes, which were also used as the loading conditions for the finite element analysis of the foot and ankle.

Figure 2 shows the GRF curves for the two touchdown patterns. Observation of the GRF curves of this subject in different touchdown modes revealed that there was a significant difference in the waveforms of the vertical ground reaction force changes.In the RFS mode, there were two peaks in the vertical GRF and the second peak was higher than the first one.The first peak appeared in the RFS with a magnitude of 1.72 times the body weight, whereas in the NRFS mode, only a single peak was observed.In the RFS mode, the first peak was 1.72 times the body weight and the second peak was 1.72 times the body weight. The maximum peak of the vertical component of the GRF was 2.5 times body weight in the RFS, and the peak of the vertical GRF was 2.68 times body weight in the NRFS.

The waveforms of the change curves of GRF in the forward and backward direction components were similar in both touchdown modes, with two maxima in opposite directions, where the negative direction maxima represented the maximum braking force in the forward and backward directions, and the positive direction maxima represented the maximum propulsive force in the forward and backward directions. Integrating the relative time of the front-back GRF change curves, respectively, we obtained the resistance impulse I_a and power impulse I_b representing braking and stirrup extension. I_a:I_b=1.85 in RFS and I_a:I_b=0.52 in NRFS, suggesting that the resistance impulse generated by touchdown with RFS is larger than the power impulse, and a larger power impulse can be obtained during touchdown with the NRFS mode.

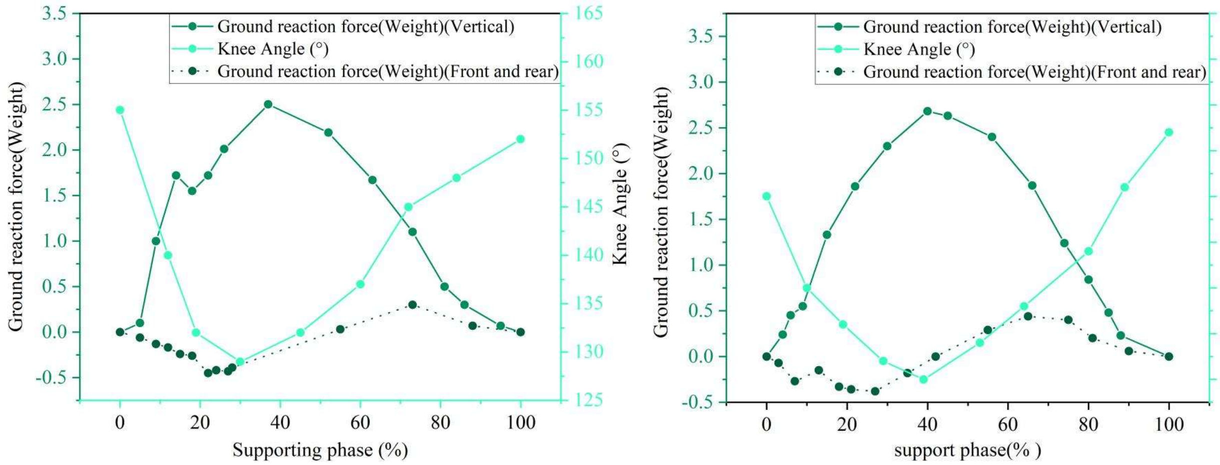

(a) GRF of RFS and lateral knee bend Angle (b) GRF of NRFS and lateral knee bend Angle

Fig. 2. GRF of two bottoming modes

3.2.3. Contact stresses on the articular surfaces of the talar heel. The articular surface cartilage of the talar heel joint is an important tissue structure of the talar joint. The results of finite element analysis showed that the maximum contact stresses of the articular surface cartilage of the talo-heel joint were very close to each other in both touchdown modes, both at the cushioning nadir and at the moment of maximum vertical GRF.

Figure 3 shows the maximum contact stress of the articular surface of the talo-heel joint in the two touchdown modes. In RFS mode, the maximum contact stress on the articular cartilage of the articular surface of the talonavicular joint appeared at the moment of maximum vertical GRF, which was 7.22 MPa. The maximum contact stress on the articular surface of the cushioning nadir was 7.14 MPa, and that at the moment of impact was 4.08 MPa.

In contrast, in the NRFS mode, the maximum peak of the talo-heel joint surface contact stress occurred at the cushioning nadir moment, which was 7.09 MPa, and the maximum vertical GRF moment in stirrups was smaller compared with that in cushioning, which was 7.01 MPa. The trend of talo-heel joint surface contact stresses was opposite to that in the RFS mode.

In addition, although the maximum contact stress on the posterior articular surface of the heel joint at the beginning of heel strike in the RFS mode was smaller compared with that at the touchdown moment in the NRFS, the contact stress on the heel joint in the RFS increased rapidly from 2.01 MPa at the moment of heel strike to 4.08 MPa at the moment of the peak of the impact in 0.05 s. The maximum vertical GRF moment was smaller compared with that at the cushioning moment.

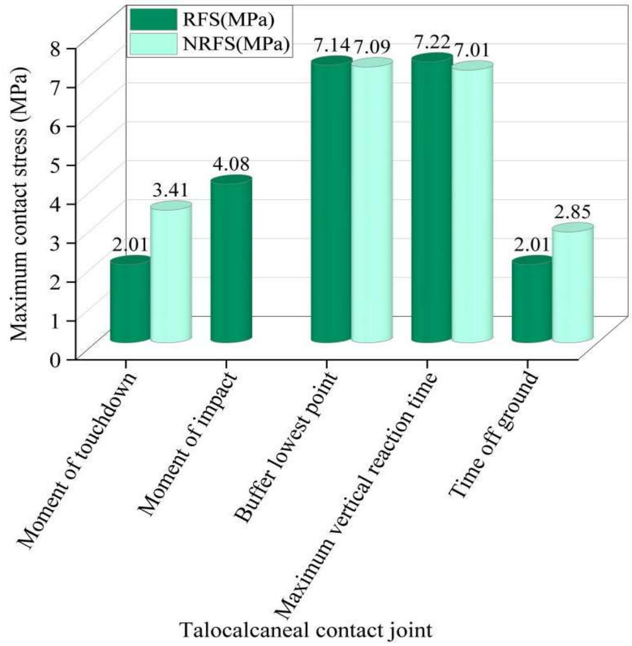

Fig. 3. Maximum contact stress of talar joint surface under two modes

4. Controlled experiments with finite element analysis in sport

The use of finite element analysis to establish foot simulation models and study the mechanical characteristics of the foot under different touchdown modes gives a detailed picture of the changes in the forces on the various tissues of the foot. This shows the application value of FEA in sports. In order to further verify that FEA can be well used to assist teachers in teaching interventions in sports, a semester-long controlled experiment was set up in this paper.

4.1. Subjects of study

This paper takes the application of finite element analysis technology in college track and field teaching as a research object.

4.2. Pedagogical experimentation

According to the requirements of track and field syllabus and teaching tasks, combined with the talent cultivation objectives of physical education majors, this study chooses the representative sport of backward high jump, and applies the finite element analysis technology to the teaching program of backward high jump in the general course of track and field of physical education majors in colleges and universities. A total of 60 subjects from Class 2201 and Class 2202 of Physical Education majoring in the Physical Education College of a university in the year 2022 were used in a 14-week (one semester) teaching experiment to further analyze the effect of the application of finite element analysis technology in the teaching of track and field in colleges and universities. The experimental class 2201 (30 students) was taught by "FEA + conventional method", while the control class 2202 (30 students) was taught by conventional method. There is no significant difference between the basic conditions of the students and the teaching conditions of the two classes except for the finite element analysis technology, which does not affect the experimental results.

4.3. *Examination of differences in body morphology and physical fitness between the two groups of students before the experiment*

Table 4 shows the comparison of body form indicators and physical quality indicators of the two groups of students before the experiment. In this paper, according to the physical and mental characteristics of students and the characteristics of the backward high jump program,and also on the basis of expert interviews,the indicators to measure the students' body morphology and physical quality were determined.The indicators of body morphology include height,weight,leg length,and the indicators of physical quality include 30-meter run,assisted one-legged jump for touching the height,standing long jump,and backward solid ball throw. It can be seen that the P-values of the two groups of students in these specific indicators before the experiment were all greater than 0.05, and there was no significant difference between the two groups of students in terms of their physical basics, which was in line with the requirements of the controlled experiment.

Table 4. Comparison of body indexes before the experiment (N=60)

Item	Experimental Group (M±SD)	Control group (M±SD)	T-value	P-value
Age (years)	18.53±0.83	18.65±1.05	-0.46	0.66
Height (cm)	181.69±4.52	181.45±5.53	0.18	0.88
Weight (kg)	68.61±5.31	71.97±7.41	-1.86	0.08
Leg length (cm)	106.69±5.39	107.77±5.66	-0.83	0.43
30 M Race (s)	4.34±0.20	4.28±0.12	1.36	0.19
Standing Long Jump (m)	2.74±0.11	2.69±0.16	1.35	0.20
Jump height (m)	1.74±0.12	1.78±0.10	-1.33	0.20
Back throw Solid Ball (m)	14.86±1.87	15.93±2.43	-1.78	0.09

Note: *P<0.05, **P<0.01

4.4. *Comparative analysis of the two groups of students' skill test scores after the experiment*

In order to verify the value of the application of finite element technology in sports, the assessment of the backward high jump program was carried out after the experiment, and each student of the two classes had two opportunities to try to jump, and the highest score was taken in the skill assessment results.

Figure 4 shows the comparison of the skill assessment scores of students in the experimental group and the control group after the experiment. Analyzing Figure 4, the average skill score of the students in the experimental group after the experiment was 90.13±4.28, and the average skill score of the students in the control group was 85.43s 3.90, and the average skill score of the students in the experimental group was better than that of the control group. The p-value of the two groups is 0.002, which is less than the level of significance of 0.01, indicating that there is a highly significant difference between the two groups of students in terms of skill performance after the experiment. Therefore, it can be inferred that the application of finite element analysis technology to the teaching of backward high jump can improve the students' motor skills.

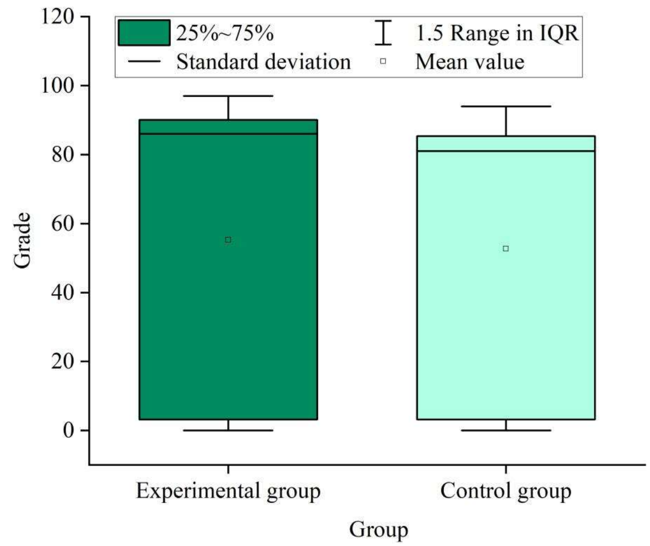

Fig. 4. Comparison of skill assessment results after the experiment

4.5. Comparative analysis of students' learning interest and initiative in the two groups after the experiment

After the experiment, 60 students in the experimental group and the control group were given a questionnaire on the teaching effect of the back-to-back high jump course. The results of the survey were quantitatively analyzed by the assignment method, in which the "strongly agree" option was assigned 5 points, the "somewhat agree" option was assigned 4 points, the "agree" option was assigned 3 points, the "not very agree" option was assigned 2 points, and the "disagree" option was assigned 1 point. Students' interest in learning and initiative were reflected in questions 1 and 2 and questions 7, 8, 13, 14 and 15 of the teaching effectiveness questionnaire, respectively.

Figure 5 shows the comparative analysis of the two groups of students' learning interest and initiative after the experiment. Comparing the data in Figure 5, the mean value of students' learning interest in the experimental group after the experiment is 4.13±0.88, and the mean value of students' learning interest in the control group is 3.69±1.10, and the mean value of students' learning interest in the experimental group is greater than that of the control group, and the P-value of the two groups of students' learning interest is 0.028, which is smaller than the significance level of 0.05, indicating that after the experiment there is a significant difference. The mean value of learning initiative of the students in the experimental group after the experiment is 3.97±1.02, and the mean value of learning initiative of the students in the control group is 3.61±1.12, the mean value of learning initiative of the students in the experimental group is greater than that of the control group, and the P-value of the two groups of students in terms of their learning initiative is 0.013, which is smaller than the level of significance of 0.05, indicating that there is a significant difference between the two groups of students in terms of their learning initiative after the experiment. The students in the experimental group are more interested in learning and have more initiative. Therefore, it can be analyzed that the application of finite element analysis technology to the teaching of backward high jump is more likely to stimulate students' learning interest and mobilize students' learning initiative.

Learning interest is a person's psychological tendency to know, explore, and acquire certain knowledge, and it is a kind of inner force to push people to seek knowledge, and the finite element analysis technology, as a kind of scientific teaching aids, is more likely to be welcomed by the students, and mobilize the students' interest in learning sports skills. When the students' interest in learning continues to improve, the students in the learning of high jump technique will be “passive learning” to “active learning”, which will improve the efficiency of listening in the classroom and the quality of practice, and will take the initiative to complete the tasks assigned by the teacher in the spare time, consciously The teacher will also take the initiative to complete the tasks assigned by the teacher and consciously practice the techniques after class.

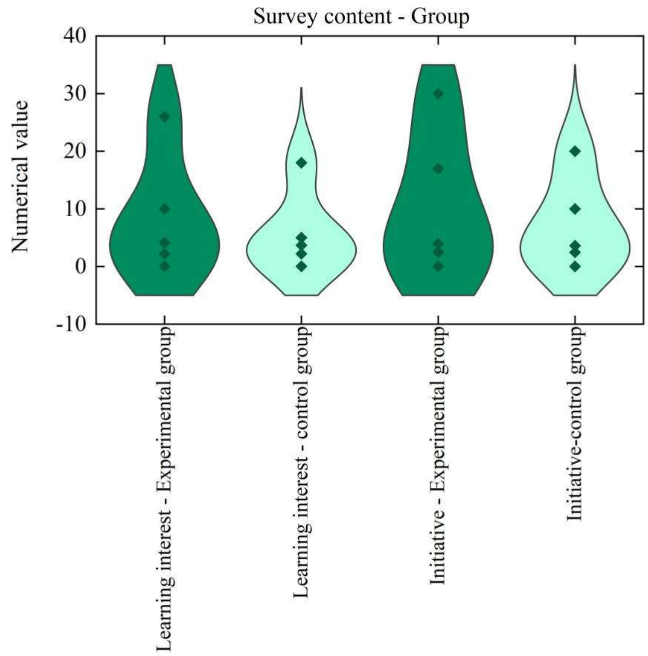

Fig. 5. Comparison of learning interest and initiative after the experiment

5. Conclusion

In this paper, finite element analysis technology is used to study the changes in the mechanical characteristics of the athlete's foot, to assist physical education teachers to provide timely intervention guidance for athletes to reduce their risk of injury, improve the standardization of their technical movements, and mobilize their motivation to play sports.

Ankle joint angle changes were analyzed in 2 touchdown modes, heel-touch and non-heel-touch.The foot flexion and extension angle change curves of the athlete's supported foot in the 2 touchdown modes were roughly similar in the posterior 75% of the support phase and differed more in the anterior 25%. The ankle range of motion was closer between 38° and 40°. The movement of the supported foot in the coronal plane showed a general tendency toward valgus, but the timing and angle of valgus varied. The ground reaction force was investigated in the 2 modes. Vertically, there were 2 peaks in the vertical ground reaction force variation for the heel-touch mode, which occurred at 1.72 times body weight and 2.5 times body weight, respectively. In contrast, the non-heel touchdown pattern showed only 1 peak at 2.68 times body weight. In the anterior-posterior direction, the 2 patterns obtained large differences in the ratios of resistance impulse I_a and power impulse I_b. $I_a : I_b$=1.85 in the heel-touch mode and $I_a : I_b$=0.52 in the nonheel-touch mode.The time sequence of the appearance of the maximal contact stress on the articular surface of the heel differed between the 2 modes of touching the ground. The contact stress in the heel-touch mode could be rapidly increased within 0.05 s, and the trend of stress change was opposite to that in the nonheel-touch mode.

Using the finite element analysis technology to model and calculate the changes in the force of various tissues of the foot of students in sports, it can be seen that the 2 modes of touchdown have a certain effect on the changes in the mechanical characteristics of the foot of students. Physical education teachers, when using finite element analysis technology to carry out controlled experiments, according to the trend of changes in the mechanical characteristics of the foot, targeted at correcting the students' foot touchdown technical movements. In order to ensure that students will not be injured or form some chronic injuries because of irregular touching in the process of sports. After a semester of experimentation, the average score of skills in the experimental class is above 90 points, and the average value of students' learning interest and initiative is about 4 points, which is significantly better than the control class. The reason for this is that the use of finite element analysis technology to personalize the intervention of students' biomechanical characteristics in physical education and sports enables students to visually see the changes in the force on their feet, increase their attention, and actively practice and correct technical movements. Moreover, the use of finite element analysis technology by physical education teachers can change the traditional teaching habit of teaching and assessing without intervening in the process of students' movement, and can also improve students' recognition of physical education and sports, and increase their participation in classroom interactions, thus forming a virtuous cycle of “analysis-intervention-improvement-participation-further analysis” and improving students' enthusiasm for physical education and sports.

Funding

This work was supported by General Science and Technology Projects of Beijing Municipal Education Commission Award (ID: KM202410009005);

The University-Industry Collaborative Education Program of the Ministry of Education of China (ID: 241200676181521).

References

[1] Vaughan, C. L. (2020). Biomechanics of sport. CRC Press.

[2] Yeadon, M. R., & Pain, M. T. G. (2023). Fifty years of performance-related sports biomechanics research. Journal of Biomechanics, 155, 111666.

[3] Glazier, P. S., & Mehdizadeh, S. (2019). Challenging conventional paradigms in applied sports biomechanics research. Sports Medicine, 49(2), 171-176.

[4] Tai, W. H., Zhang, R., & Zhao, L. (2023). Cutting-Edge Research in Sports Biomechanics: From Basic Science to Applied Technology. Bioengineering, 10(6), 668.

[5] Hughes, G. T., Camomilla, V., Vanwanseele, B., Harrison, A. J., Fong, D. T., & Bradshaw, E. J. (2024). Novel technology in sports biomechanics: Some words of caution. Sports Biomechanics, 23(4), 393-401.

[6] Penichet-Tomas, A. (2024). Applied Biomechanics in Sports Performance, Injury Prevention, and Rehabilitation. Applied Sciences, 14(24), 11623.

[7] Weiss, K., & Whatman, C. (2015). Biomechanics associated with patellofemoral pain and ACL injuries in sports. Sports medicine, 45, 1325-1337.

[8] Barua, R. (2025). Unleashing Human Potential: Exploring the Advantage of Biomechanics in Sport Performance. In Global Innovations in Physical Education and Health (pp. 409-436). IGI Global.

[9] Navarro, E., Navandar, A., Veiga, S., & San Juan, A. F. (2021). Applied biomechanics: Sport performance and injury prevention. Applied Sciences, 11(9), 4230.

[10] Forte, P., & Teixeira, J. E. (2023, March). Exercise Biomechanics for Health: Evaluating Lifelong Activities for Well-Being. In Healthcare (Vol. 11, No. 6, p. 900). MDPI.

[11] Forte, P., Neiva, H. P., & Marinho, D. A. (2021). Sports biomechanics: monitoring health and performance. Journal of Men’s Health, 1.

[12] Najafian Razavi, M., & Rezaei, M. (2023). Comparison of Biomechanical Models for Roundhouse Kicking in Skilled Martial Arts Students of Taekwondo and Wushu (Sanda). Journal of Sport Biomechanics, 9(3), 220-232.

[13] Kumar, S., & Das, R. (2024). Championing Olympic Excellence: A Bibliometric Analysis of Biomechanics Impacting Tennis Performance on the World Stage. Physical Education Theory and Methodology, 24(3), 494-503.

[14] Wong, D. W. C., Lee, W. C. C., & Lam, W. K. (2020). Biomechanics of table tennis: A systematic scoping review of playing levels and maneuvers. Applied Sciences, 10(15), 5203.

[15] Lam, W. K., Kan, W. H., Chia, J. S., & Kong, P. W. (2022). Effect of shoe modifications on biomechanical changes in basketball: A systematic review. Sports Biomechanics, 21(5), 577-603.

[16] Nazari, F., & Fatahi, A. (2023). Football Biomechanics and Performance Enhancement: A Systematic Review. Journal of Sport Biomechanics, 9(3), 252-270.

[17] Li, M. (2024). Research on the application of biomechanics analysis in optimizing physical education movement techniques. Molecular & Cellular Biomechanics, 21(3), 496-496.

[18] Potop, V., Mihailescu, L. E., Mihaila, I., Zawadka-Kunikowska, M., Jagiello, W., Chernozub, A., ... & Ascinte, A. (2024). Applied biomechanics within the Kinesiology discipline in higher education. Physical Education of Students, 28(2), 106-119.

[19] Ying, W., & Huang, W. (2021). Research on Methods of Improving Teaching Efficiency of Physical Training Based on Sports Biomechanics. Curriculum and Teaching, 4, 14-18.

[20] Kartiko, D. C. (2018, April). Revealing physical education students' misconception in sport biomechanics. In Journal of Physics: Conference Series (Vol. 1006, No. 1, p. 012040). IOP Publishing.